Sensitive method for measuring third order nonlinearities in compact dielectric and hybrid plasmonic waveguides

F. J. Diaz,[1,5] T. Hatakeyama,[3] J. Rho,[3] Y. Wang,[3] K. O'Brien,[3] X. Zhang,[3,4] C. Martijn de Sterke,[1,2] B. T. Kuhlmey,[1,2] and S. Palomba[1,6]

[1] *Institute of Photonics and Optical Science (IPOS), School of Physics, The University of Sydney, NSW 2006, Australia*

[2] *Center for Ultrahigh Bandwidth Devices for Optical Systems (Cudos), Australia*

[3] *NSF Nanoscale Science and Engineering Center (NSEC), 3112 Etcheverry Hall, University of California, Berkeley, California 94720, USA*

[4] *Materials Sciences Division, Lawrence Berkeley National Laboratory, Berkeley, California 94720, USA*

[5] *f.diaz@physics.usyd.edu.au*

[6] *stefano.palomba@sydney.edu.au*

Abstract: We demonstrate a sensitive method for the nonlinear optical characterization of micrometer long waveguides, and apply it to typical silicon-on-insulator nanowires and to hybrid plasmonic waveguides. We demonstrate that our method can detect extremely small nonlinear phase shifts, as low as $7.5 \cdot 10^{-4}$ rad. The high sensitivity achieved imparts an advantage when investigating the nonlinear behavior of metallic structures as their short propagation distances complicates the task for conventional methods. Our results constitute the first experimental observation of $\chi^{(3)}$ nonlinearities in the hybrid plasmonic platform and is important to test claims of hybrid plasmonic structures as candidates for efficient nonlinear optical devices.

OCIS codes: (120.0120) Instrumentation, measurement, and metrology; (230.4320) Nonlinear optical devices.

References and links

1. B. Booth, B. Bottoms, S. Buchter, D. Butler, T. Bowen, G. Celler, Y. Chen, D. Evans, L. Giovane, M. Glick, R. Grzybowski, B. Hemenway, L. Kimerling, L. Liao, H. Lui, J. Michel, J. Mu, R. Otte, P. Popescu, M. Romagnoli, L. Smith, V. Stojanovic, M. Tan, M. Taubenblatt, M. Tryson, C. Weaver, and T. Yamamoto, "On-Board Optical Interconnection Digest," in CTR III TWG Report #32013, Community Technology Roadmap (CTR, 2013)
2. D. A. B. Miller, "Are optical transistors the logical next step?" Nat. Photonics **4**(1), 3–5 (2010).
3. J. A. Kash, "Leveraging optical interconnects in future supercomputers and servers," in *16th IEEE Symposium on High Performance Interconnects* (IEEE, 2008), pp. 190-194.
4. H. K. Tsang and Y. Liu, "Nonlinear optical properties of silicon waveguides," Semicond. Sci. Technol. **23**(6), 064007 (2008).
5. J. Y. Lee, L. Yin, G. P. Agrawal, and P. M. Fauchet, "Ultrafast optical switching based on nonlinear polarization rotation in silicon waveguides," Opt. Express **18**(11), 11514–11523 (2010).
6. V. Shahraam Afshar, T. M. Monro, and C. M. de Sterke, "Understanding the contribution of mode area and slow light to the effective Kerr nonlinearity of waveguides," Opt. Express **21**(15), 18558–18571 (2013).
7. C. Ciracì, R. T. Hill, J. J. Mock, Y. Urzhumov, A. I. Fernández-Domínguez, S. A. Maier, J. B. Pendry, A. Chilkoti, and D. R. Smith, "Probing the Ultimate Limits of Plasmonic Enhancement," Science **337**(6098), 1072–1074 (2012).
8. C. Haffner, W. Heni, Y. Fedoryshyn, J. Niegemann, A. Melikyan, D. L. Elder, B. Baeuerle, Y. Salamin, A. Josten, U. Koch, C. Hoessbacher, F. Ducry, L. Juchli, A. Emboras, D. Hillerkuss, M. Kohl, L. R. Dalton, C. Hafner, and J. Leuthold, "All-plasmonic Mach–Zehnder modulator enabling optical high-speed communication at the microscale," Nat. Photonics **9**(8), 525–528 (2015).
9. A. Melikyan, L. Alloatti, A. Muslija, D. Hillerkuss, P. C. Schindler, J. Li, R. Palmer, D. Korn, S. Muehlbrandt, D. Van Thourhout, B. Chen, R. Dinu, M. Sommer, C. Koos, M. Kohl, W. Freude, and J. Leuthold, "High-speed plasmonic phase modulators," Nat. Photonics **8**(3), 229–233 (2014).
10. M. Kauranen and A. V. Zayats, "Nonlinear plasmonics'," Nat. Photonics **6**(11), 737–748 (2012).

#253928 Received 17 Nov 2015; revised 18 Dec 2015; accepted 20 Dec 2015; published 7 Jan 2016

11. J. B. Khurgin and G. Sun, “Plasmonic enhancement of the third order nonlinear optical phenomena: figures of merit,” Opt. Express **21**(22), 27460–27480 (2013).
12. R. F. Oulton, V. J. Sorger, D. A. Genov, D. F. P. Pile, and X. Zhang, “A hybrid plasmonic waveguide for subwavelength confinement and long-range propagation,” Nat. Photonics **2**(8), 496–500 (2008).
13. Y. Bian and Q. Gong, “Low-loss hybrid plasmonic modes guided by metal-coated dielectric wedges for subwavelength light confinement,” Appl. Opt. **52**(23), 5733–5741 (2013).
14. Y. Bian and Q. Gong, “Deep-subwavelength light confinement and transport in hybrid dielectric-loaded metal wedges,” Laser Photonics Rev. **8**(4), 549–561 (2014).
15. Y. Bian and Q. Gong, “Tuning the hybridization of plasmonic and coupled dielectric nanowire modes for highperformance optical waveguiding at sub-diffraction-limited scale,” Sci. Rep. **4**, 6617 (2014).
16. J. T. Kim, J. J. Ju, S. Park, M. S. Kim, S. K. Park, and S. Y. Shin, “Hybrid plasmonic waveguide for low-loss lightwave guiding,” Opt. Express **18**(3), 2808–2813 (2010).
17. Y. Bian, Z. Zheng, X. Zhao, Y. Su, L. Liu, J. Liu, J. Zhu, and T. Zhou, “Guiding of Long-Range Hybrid Plasmon Polariton in a Coupled Nanowire Array at Deep-Subwavelength Scale,” Photonics Technol. Lett. **24**(15), 1279–1281 (2012).
18. Y. Ma, G. Farrell, Y. Semenova, and Q. Wu, “Hybrid nanowedge plasmonic waveguide for low loss propagation with ultra-deep-subwavelength mode confinement,” Opt. Lett. **39**(4), 973–976 (2014).
19. S. Aldawsari and B. R. West, “Hybrid plasmonic waveguides for nonlinear applications,” in Photonics Global Conference (PGC, 2012).
20. A. Pitilakis and E. E. Kriezis, “Highly nonlinear hybrid silicon-plasmonic waveguides: analysis and optimization,” J. Opt. Soc. Am. B **30**(7), 1954–1965 (2013).
21. K.Y. Wang, and A.C. Foster. “Optimization of CMOS-Compatible Hybrid Plasmonic Waveguides for Nonlinear Applications,” in *Advanced Photonics OSA Technical Digest* (Optical Society of America, 2011), paper JTuB15.
22. K. Narayanan and S. F. Preble, “Optical nonlinearities in hydrogenated-amorphous silicon waveguides,” Opt. Express **18**(9), 8998–9005 (2010).
23. E. Dulkeith, Y. A. Vlasov, X. Chen, N. C. Panoiu, and R. M. Osgood, Jr., “Self-phase-modulation in submicron silicon-on-insulator photonic wires,” Opt. Express **14**(12), 5524–5534 (2006).
24. Y. Shoji, T. Ogasawara, T. Kamei, Y. Sakakibara, S. Suda, K. Kintaka, H. Kawashima, M. Okano, T. Hasama, H. Ishikawa, and M. Mori, “Ultrafast nonlinear effects in hydrogenated amorphous silicon wire waveguide,” Opt. Express **18**(6), 5668–5673 (2010).
25. N. Dudovich, D. Oron, and Y. Silberberg, “Single-pulse coherently controlled nonlinear Raman spectroscopy and microscopy,” Nature **418**(6897), 512–514 (2002).
26. W. Min, S. Lu, M. Rueckel, G. R. Holtom, and X. S. Xie, “Near-Degenerate Four-Wave-Mixing Microscopy,” Nano Lett. **9**(6), 2423–2426 (2009).
27. H. Suchowski, K. O’Brien, Z. J. Wong, A. Salandrino, X. Yin, and X. Zhang, “Phase Mismatch–Free Nonlinear Propagation in Optical Zero-Index Materials,” Science **342**(6163), 1223–1226 (2013).
28. G. P. Agrawal, *Nonlinear Fiber Optics*, 4th ed. (Academic Press, 2006), Ch. 4.
29. G. P. Agrawal, *Nonlinear Fiber Optics*, 4th ed. (Academic Press, 2006), Ch. 2.
30. R. Dekker, E. J. Klien, J. Niehusmann, M. Först, F. Ondracek, J. Ctyroky, N. Usechak, and A. Dressen, “Self phase modulation and stimulated raman scattering due to high power femtosecond pulse propagation in silicon-on-insulator waveguides,” in Proceedings Symposium IEEE/LEOS Benelux Chapter (IEEE, 2005), pp. 197-200.
31. A. Präkelt, M. Wollenhaupt, C. Sarpe-Tudoran, A. Assion, and T. Baumert, “Filling a spectral hole via self-phase modulation,” Appl. Phys. Lett. **87**(12), 121113 (2005).
32. D. Vermeulen, K. V. Acoleyen, S. Ghosh, S. Selvaraja, W. A. D. De Cort, N. A. Yebo, E. Hallynck, K. De Vos, P. P. P. Debackere, P. Dumon, W. Bogaerts, G. Roelkens, D. Van Thourhout, and R. Baet, “Efficient tapering to the fundamental quasi-TM mode in asymmetrical waveguides,” in 15th European conference on Integrated Optics (ECIO, 2010).
33. W. Bogaerts, R. Baets, P. Dumon, V. Wiaux, S. Beckx, D. Taillaert, B. Luyssaert, J. Van Campenhout, P. Bienstman, and D. Van Thourhout, “Nanophotonic waveguides in silicon-on-insulator fabricated with CMOS technology,” J. Lightwave Technol. **23**(1), 401–412 (2005).
34. D. Taillaert, F. Van Laere, M. Ayre, W. Bogaerts, D. Van Thourhout, P. Bienstman, and R. Baets, “Grating couplers for coupling between optical fibers and nanophotonic waveguides,” Jpn. J. Appl. Phys. **45**(8A), 6071–6077 (2006).
35. B. Esembeson, M. L. Scimeca, T. Michinobu, F. Diederich, and I. Biaggio, “A high-optical quality supramolecular assembly for third-order nonlinear optics,” in *Conference on Lasers and ElectroOptics/International Quantum Electronics Conference* (CLEO, 2009), paper JWA120.

1. Introduction

The sophistication and need for integrated optical devices is rapidly increasing due to its importance to future communications technology. The demands of data bandwidth together with restrictions on power consumption are driving the replacement of electronic components by optical counterparts [1]. Current industrial focus aims to bring optical interconnects as close as physically possible to the data processing unit, however future trends may encompass the complete replacement of the electronic circuit [2, 3]. The advent of all optical

#253928 Received 17 Nov 2015; revised 18 Dec 2015; accepted 20 Dec 2015; published 7 Jan 2016

data processing will require adequate development of integrated nonlinear optical devices, which in turn require strong light-matter interactions, low losses and a small physical footprint.

The current leading platform for nonlinear optical devices is silicon nanophotonics owing to its CMOS compatibility, low loss, high third-order susceptibility $\chi^{(3)}$, and large index contrast which enables a relatively strong field confinement [4, 5]. Field confinement has proven essential in achieving large nonlinear effects, as it enhances light-matter interactions while maintaining low power requirements [6]. However, silicon nanowires are purely dielectric and are therefore inherently restricted by the diffraction limit. In contrast, plasmonic structures can surpass this limit and can compress the field into subwavelength regions. Strong field enhancements of up to three orders of magnitudes have been demonstrated [7]. This characteristic is what makes plasmonics an attractive platform for integrated nonlinear optics [8, 9]. However, the enhancement comes at the cost of increased linear losses, which may ultimately rule out plasmonics for practical nonlinear applications [10, 11].

In an effort to mitigate plasmonic losses, the hybrid plasmonic waveguide (HPWG) was proposed by Oulton et al. [12] as an alternative plasmonic structure. HPWGs, which combine elements of dielectric and plasmonic waveguides, have been shown to retain considerable field compression while lowering propagation losses attributed to plasmonics [13, 14]. This finding has given rise to numerous computational studies highlighting the properties of the hybrid platform over a range of different geometries [15–18]. Although hybrid structures do improve propagation losses compared to purely plasmonic waveguides, the propagation length remains short compared to dielectric waveguides. It remains unclear whether the HPWG will in fact be useful for nonlinear optical applications [19–21].

To date limited experimental work has been carried out. In order to better gauge the real potential of hybrid plasmonic structures for nonlinear optics, more experimental evidence is needed. However, nonlinear measurements of such short waveguides are difficult with conventional techniques. First, the short physical length of these waveguides complicates the separation of input and output power. Secondly, short waveguides typically lead to weak nonlinear signals, unless this is offset by large nonlinearity. In practice a weak nonlinear signal may be coherently strengthened by extending the waveguide's length. Indeed typical silicon-on-insulator (SOI) waveguides for nonlinear optical experiments are a few millimeters in length [22–24], clearly this option is unavailable for the short propagation lengths in plasmonic waveguides. Thus measuring a nonlinear phase shift over micrometer lengths requires an extremely sensitive method.

With these restrictions in mind we demonstrate a method for measuring the nonlinear phase shift of micrometer-length waveguides. This may be used as a means to evaluate claims of enhanced nonlinearities in newly proposed waveguide structures, particularly those with plasmonic attributes. Our method is an adaptation of a technique used for nonlinear microscopy [25–27], which we repurpose to achieve a sensitive, background-free nonlinear measurement of micrometer short waveguides. As proof of the method's reliability, we report a study of SOI nanowires with differing lengths. We also apply our method to a set of hybrid plasmonic waveguides, which constitute the first nonlinear experimental demonstration of nonlinear optical generation on such a platform.

2. Method

2.1 Concept

Figure 1 conceptualizes the key points of our method. A laser source provides a pulse centered at a wavelength λ_c. The pulse is spectrally truncated such that the long-wavelengths (i.e., $\lambda > \lambda_t$) are removed, forming an abrupt cut in the spectrum. This truncated pulse is then launched into the waveguide, where it spectrally broadens due to self-phase modulation (SPM), originating from the waveguide's cubic nonlinearity [28]. Subsequently, a long pass filter is applied to remove all wavelengths with $\lambda < \lambda_f$, where $\lambda_f > \lambda_t$, ensuring that only

#253928 Received 17 Nov 2015; revised 18 Dec 2015; accepted 20 Dec 2015; published 7 Jan 2016

frequencies which were nonlinearly generated are detected. In short, the combined use of the spectrally truncated pulse and a sharp-edged long pass filter creates a background-free condition which improves the signal to noise ratio (SNR) and enables weak signal detection.

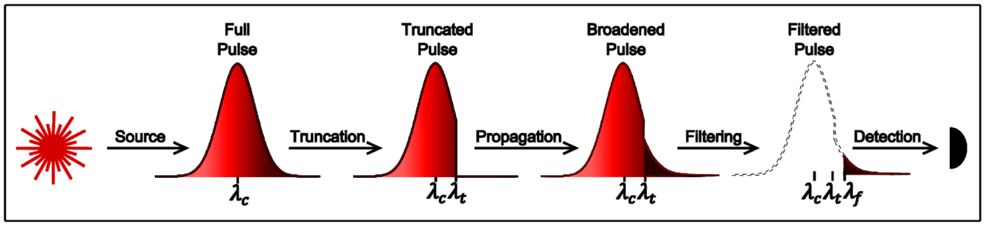

Fig. 1. Conceptual illustration of the method. A source provides a pulse centred at λ_c. The pulse is truncated at λ_t, and is then broadened during propagation. The pulse is filtered at λ_f.

To optimize the SNR, care should be taken in choosing the parameters λ_c, λ_t, and λ_f. We first consider the wavelength offset $\Delta_{tc} = (\lambda_t - \lambda_c)$. If this parameter is chosen to be too large, considerable spectral broadening is needed to observe a nonlinear signal. In addition, as discussed below, an enhancement leading to a strong nonlinear signal will be lost. In contrast, if chosen to be too small, the pulse looses so much energy that the broadening effect of the SPM weakens.

Now consider the offset $\Delta_{ft} = (\lambda_f - \lambda_t)$. This offset needs to be positive in order to avoid leakage of the original pump, which would ruin the background-free condition. Though one could in principle choose $\lambda_f = \lambda_t$, neither the truncated edge λ_t nor the filter edge λ_f are perfect step functions which would allow part of the original pump pulse to reach the detector. Consequently there must be a minimum distance between the two to prevent this leakage. If this offset is too large then this results in a reduced signal.

2.2 Implementation

Figure 2 shows a schematic of our complete experimental setup. A femtosecond pulse with a center wavelength $\lambda_c = 1305$ nm was generated by an optical parametric oscillator (Coherent Inc.), with its average power and polarization controlled by a half-waveplate and polarizer. The pulse is directed into a 4f pulse-shaper (see inset Fig. 2c) set to minimize linear chirp while simultaneously removing wavelengths $\lambda > \lambda_t = 1311$ nm. As approximately 30% of the power was removed the resulting pulse is effectively truncated without causing too much temporal broadening. The truncated pulse spectrum (inset Fig. 2a) and its corresponding pulse-width measured to be 207 fs (inset Fig. 2b), were independently verified by a spectrometer and autocorrelation measurement. The sample was mounted on an XYZ nanopositioner, installed on a commercial inverted microscope. The photonic devices are sufficiently small to fit comfortably within the field of view of a 100x NIR Olympus objective (N.A. 0.85) (see inset Fig. 2d). The pulse, which may be further attenuated by a removable neutral density filter of OD = 5.62, was launched onto the sample objective and coupled into the waveguide where propagation and spectral broadening ensued. The output was collected by the same objective, and a combination of spectral and spatial filtering was applied prior to detection (see inset Fig. 2e). Two Semrock RazorEdge long-pass filters were used to eliminate wavelengths $\lambda < \lambda_f = 1328$ nm, but may be removed when no spectral filtering is required. Spatial filtering was implemented by carefully placing an aperture at the image plane, physically blocking all light which does not originate from the waveguide's output. This ensures that only the nonlinear signal generated within the waveguide would be collected. The signal was analyzed by an Imaging Spectrometer (IsoPlane - Princeton Instruments) equipped with an ultra-low noise near-infrared (InGaAs) camera (NIRvana - Princeton Instruments) with a response time of 100 ms.

#253928 Received 17 Nov 2015; revised 18 Dec 2015; accepted 20 Dec 2015; published 7 Jan 2016

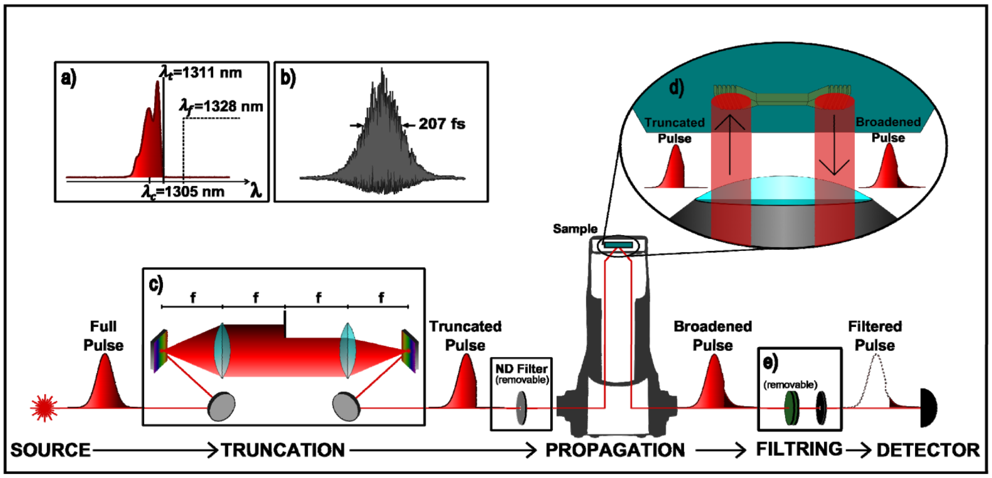

Fig. 2. Schematic of the complete experimental implementation. a) Spectral measurement of the truncated pulse λ_c = 1305 nm, λ_t = 1311 nm, λ_f = 1328 nm; dips in spectra are due to a Fabry-Perot cavity. b) Two photon autocorrelation of the truncated pulse; pulsewidth is 207 fs and shows no observable chirp. c) 4f pulse shaper set to form the truncated pulse. d) Incoupling/Outcoupling scheme to/from waveguide sample using a 100x NIR Olympus objective (N.A. 0.85). e) Spectral and spatial filtering using two Semrock RazorEdge long-pass filters and an aperture at the image plane, respectively.

As described in more detail in Section 3, the samples consist of an input grating coupler, a waveguide and an output grating coupler. As consistent coupling is essential to achieve reliable results, the input beam was set to an incident angle and remained unaltered for all following measurements. Instead, the samples themselves were moved into position which was determined by maximizing their transmitted light. For clarity, in the following section, we express all average powers with the use of angeled brackets (e.i., $\langle P\rangle$) and all peak powers without them (e.i., P).

The average power launched onto the input grating $\langle P_{IN}\rangle$ can be controlled in two ways: by a half-waveplate/polarizer pair and by a neutral density filter (NDF). The half-waveplate/polarizer pair permits a continuous control of the attenuation, with which we set six discrete values of $\langle P_{IN}\rangle$ = 21 mW, 28 mW, 35 mW, 42 mW, 49 mW, and 56 mW for our laser and without a nuetral density filter. The NDF has a transmission of 2.4×10^{-6} and permits an additional fixed attenuation of $\langle P_{IN}\rangle$. We perform two sets of measurements for each value of $\langle P_{IN}\rangle$: our *linear* measurements are taken with the NDF in place, our *nonlinear* measurements are taken with this filter removed. We now discuss these in turn.

In our linear experiments we remove the long pass filter, place the NDF, and measure the average power at the output of the grating $\langle P_l\rangle$. From simulations we estimate the gratings to have a coupling efficiency of 33%, which allows us to determine the average power at the end of the waveguide $\langle P_L\rangle$. This power is related to the average power at the waveguide's input $\langle P_o\rangle$ by the propagation losses; in the case of a lossless waveguide $\langle P_L\rangle = \langle P_o\rangle$. The ratio $\langle P_o\rangle/\langle P_{IN}\rangle$ then gives the efficiency of the input coupling. For our setup this efficiency is 0.001%, considerably lower than the output coupling efficiency. The input coupling efficiency is given by two factors. The innate coupling efficiency of the grating (33%) and the high numerical aperture of the lens which couples into higher modes that do not enter the nonlinear waveguide. All average powers can be converted to peak powers by knowing the laser's repetition rate, pulse length and pulse shape. In particular, we convert P_L the peak power of the pulses at the end of the waveguide.

In our nonlinear experiments we remove the NDF, put the long-pass filter in place, and measure the average power at the output of the grating $\langle P_{nl}\rangle$ all of which is generated nonlinearly. As before, accounting for a grating coupling efficiency of 33%, we determine

#253928 Received 17 Nov 2015; revised 18 Dec 2015; accepted 20 Dec 2015; published 7 Jan 2016

the average nonlinear power at the end of the waveguide $\langle P_{NL} \rangle$. We do not calculate peak power since the pulse shape is severely distorted by the long-pass filter.

In this manner we obtain six correlated values of $\langle P_{NL} \rangle$ and P_L, which correspond to the six values of $\langle P_{IN} \rangle$. $\langle P_{NL} \rangle$ represents the nonlinear signal generated and P_L represents the peak power the waveguide's end. To avoid any unwanted changes in the system we measure $\langle P_{NL} \rangle$ and P_L consecutively for each value of $\langle P_{IN} \rangle$. In Section 3 we plot $\langle P_{NL} \rangle$ versus P_L and compare to simulations.

2.3 Theory

Pulse propagation through a waveguide can be simulated numerically by solving the nonlinear Schrödinger equation (Eq. (1)) via the split step Fourier method [29].

$$\frac{\partial A(z,t)}{\partial z} = -\frac{\alpha}{2} A(z,t) - i\frac{\beta}{2}\frac{\partial^2 A(z,t)}{\partial t^2} + i\gamma \left|A(z,t)\right|^2 A(z,t) \tag{1}$$

Here, A(z,t) is the field envelope amplitude, α is the linear loss, β the quadratic waveguide dispersion, and γ the nonlinear parameter. Dispersion and higher order dispersion effects may be neglected as the calculated dispersion length of ~15 mm greatly exceeds the waveguide length of ~10 μm, while the short pulsewidth of ~200 fs permits us to neglect free carrier effects [28]. Intrapulse Raman scattering may also be neglected as crystalline silicon has a Raman gain spectrum too sharp to induce the effect [30].

Figure 3 compares the propagation of a full pulse to that of a truncated pulse, illustrating how each is affected by SPM. We show the spectral evolution of each corresponding pulse at four different values of the nonlinear phase shift, which may be calculated as $\Delta\phi_{NL} = \gamma PL$. Where P is the pulse peak power and L the propagation length; in the presence of loss L must by adjusted accordingly [28].

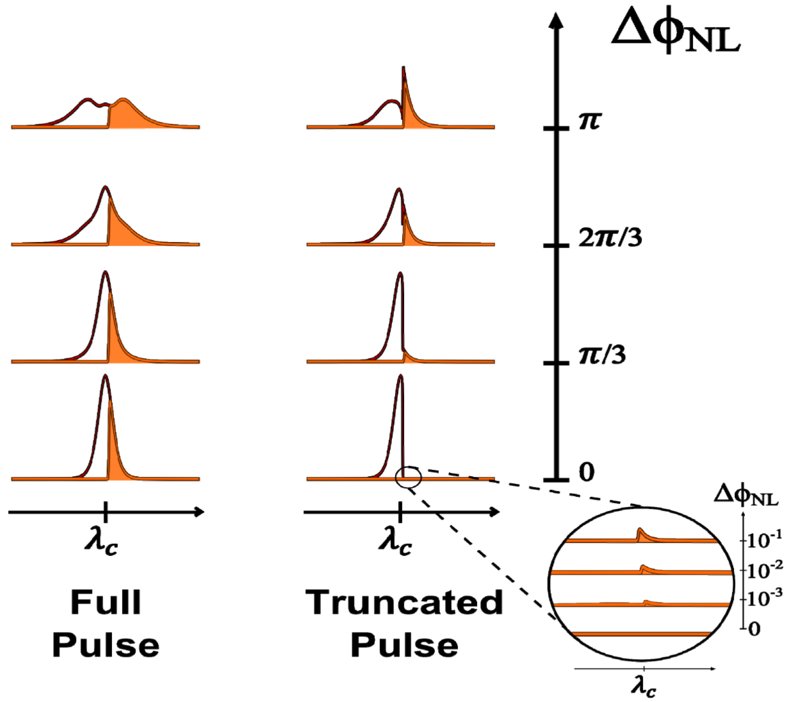

Fig. 3. SPM pulse propagation in the presence of a cubic nonlinearity for different nonlinear phase shifts; Left: Full sech pulse, Right: Spectrally truncated sech pulse. The area beneath the orange curve corresponds to the wavelengths which pass through the filter. The inset (not to scale) illustrates the measured signal for the small nonlinear phase shifts in our experiment.

#253928 Received 17 Nov 2015; revised 18 Dec 2015; accepted 20 Dec 2015; published 7 Jan 2016

In contrast to the full pulse, the truncated pulse is clearly background free; a strong spectral response is observed at $\Delta\phi_{NL} = \pi$ near the truncated wavelength λ_t which is absent for the full pulse. We find this SPM enhancement effect to be in accordance with the argument outlined by Präkelt et al. [31]. A truncated pulse can be interpreted as the sum of a full pulse and the missing segment delayed with a π phase shift. If the missing segment's bandwidth is considerably smaller than the full pulse, then in the time domain this results in a pulse propagating alongside a quasi-continuous wave (QCW). In contrast to the pulse, the QCW has a low peak power and is unaffected by SPM. Therefore as the pulse propagates and accumulates a nonlinear phase through SPM, it eventually constructively interferes with the QCW, resulting in the strong spectral peak. As the offset Δ_{tc} increases, the truncated edge λ_t approaches the pulse tail. Consequently the corresponding QCW drops in intensity and the interference effect is weakened. Thus, to achieve SPM enhancement, Δ_{tc} should not be chosen to be too large. We note that, as is expected from an interference effect, the maximum spectral peak is found at $\Delta\phi_{NL} = \pi$. As our measured phase shifts are far from that value, the benefits from this enhancement to our study is small.

3. Results

The method was tested by measuring an array of silicon waveguides fabricated on a single SOI chip. Subsequently, we performed the first reported experimental measurements to date on HPWGs.

3.1 SOI

Inset Fig. 4a shows a scanning electron microscope (SEM) image of a 10 μm long SOI waveguide, which consists of a silicon nanowire, two linear tapers and two grating couplers. The chip contains six nominally exact replicas of every structure to allow for averaging over coupling errors and fabrication imperfections The nanowire waveguide has a cross-section of 350 nm x 340 nm, and two waveguides of differing lengths were studied: 5 μm and 10 μm. At either end of the waveguide are located two linear tapers which lead out into a pair of grating couplers 4 μm wide and 5.9 μm long. The gratings are fully etched up to the oxide layer and possess a height of 340 nm, a period of 590 nm, and a duty cycle of 65%. This exact structure will be used as the base device for fabricating the HPWG samples detailed in the following section.

At a wavelength of 1305 nm the waveguide supports three guided modes: TE, TM and HE_{01}. Through polarization control and excitation symmetry, we may selectively launch the fundamental TM mode (inset Fig. 4b). Our taper was designed such that mode conversion [32] is negligible.

As the field is strongest in the nanowire, we consider it the predominant source of nonlinearity and ignore contributions from the tapers and gratings. Given the silicon waveguide's mode, the nonlinear coefficient was calculated to be $\gamma = 1.59\cdot10^{-4}$ $(\mu\text{m}\cdot\text{W})^{-1}$ using the full vectorial model of Afshar V. et al. [6], the dispersion was calculated to be $\beta = -2.74$ $(\text{fs}^2/\mu\text{m})$, and the absorption α was taken to correspond to 3 dB/cm as a moderate loss for silicon waveguides [33]. Due to the waveguide's short length, the linear loss and dispersion do not significantly affect the results but have been included in the simulations.

In order to compare simulations to experimental data, the coupling efficiency of the grating must be considered. Employing a frequency eigenmode expansion technique (CAMFR [34]) we estimate a coupling efficiency of 33%, a back reflection of 32%, and 34% power lost into the substrate. Thus, while the grating permits light to couple into the waveguide, it also creates considerable back reflection. This results in a weak Fabry-Perot effect, which can be ignored in our samples because the cavity round trip time is considerably longer than the pulse duration.

Figure 4 shows the nonlinear signal $\langle P_{NL}\rangle$ versus the pump peak power within the waveguide P_L, along with the associated simulations. Every data point represents the value of $\langle P_{NL}\rangle$ and P_L averaged over the replicated waveguides. The error bars are the respective

#253928 Received 17 Nov 2015; revised 18 Dec 2015; accepted 20 Dec 2015; published 7 Jan 2016

standard deviations. Each curve contains six data points corresponding to different values of <P_{IN}>: From left to right the points for each curve correspond to 21 mW, 28 mW, 35 mW, 42 mW, 49 mW, respectively. However, as discussed in Section 2.2, only a fraction of this power enters the waveguide (~0.001).

In order to demonstrate the method's reliability the measurements were repeated three times over the course of three days, which we plot with different colors. Although the total power coupled into the waveguide varies from day to day, which we attribute to slight variations in the laser source, on a given day the standard deviation is low and the curve's overall trend remains. In addition, we find excellent agreement between measurement and the simulations.

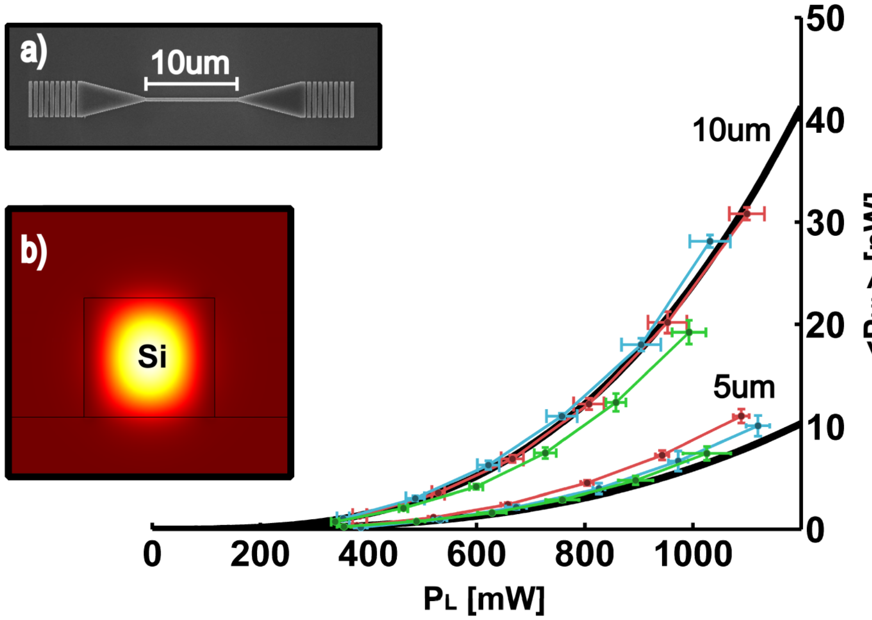

Fig. 4. Nonlinear signal generated by SOI waveguides of two differing length: 10 μm and 5 μm. Each coloured data set represents a repeated measurement performed on a separate day. The solid line is the theoretical fit. a) SEM of the standard 10 μm SOI photonic devices. b) SOI cross-section overlapped with TM mode power profile.

The pulse's width, spectra and chirp used for our simulations were independently obtained using autocorrelation and spectral measurements, shown in Fig. 2a and Fig. 2b. Having characterized the longpass filter edge and calculated the nonlinear parameter, we are left with the grating efficiency as an adjustable parameter to fit the experimental data. We found an efficiency of 32% best fits our data, which matches well with the CAMFR simulated value of 33%. These experimental results demonstrate that we can measure, and distinguish, the nonlinear signals from 5 μm and 10 μm short silicon waveguides. We calculate the minimum observable nonlinear signal, at P_L = 1000 mW and L = 5 μm, to have a nonlinear phase shift as small as $\Delta\phi_{NL} = 7.9\cdot10^{-4}$ rad.

3.2 HPWG

As before, all waveguides were fabricated on a single SOI chip containing replicas of every structure. The HPWG structure consists of the identical silicon photonic device described in the previous section (inset Fig. 4a); with a thin layer of Silicon Nitride (Si_3N_4) sandwiched between a 100 nm gold (Au) film and the silicon nanowire (inset Fig. 5b). In this set of measurements, one control SOI waveguide and two HPWG structures where measured with

#253928 Received 17 Nov 2015; revised 18 Dec 2015; accepted 20 Dec 2015; published 7 Jan 2016

different Si_3N_4 layer thickness: 5 nm and 10 nm. All waveguides measured have a length of 10 μm.

Figure 5 shows the data taken from the SOI control and HPWGs in the same format, and for the same values of $\langle P_{IN} \rangle$, as in Fig. 4. SEM images show a slight misalignment of the gold layer with respects to the silicon nanowire. This causes alterations in the desired mode profile, which creates uncertainties in the calculation of γ, as well as uncertainties in the excitation efficiencies of the two supermodes (a "symmetric-like" mode and an "asymmetric-like" mode). As these issues may not be reliably included in our simulations we do not show a theoretical curve as done in Fig. 4, instead we take a black-box approach for a qualitative analysis of the results and only compare the nonlinear signal generated for the same $\langle P_{IN} \rangle$. As an example we take the last data point of each curve in Fig. 5, marked by the dashed lines, which pertain to $\langle P_{IN} \rangle$ = 49 mW. Looking at the corresponding values of $\langle P_{NL} \rangle$ we directly compare the nonlinear phase shift achieved, which takes into account the effects of propagation losses.

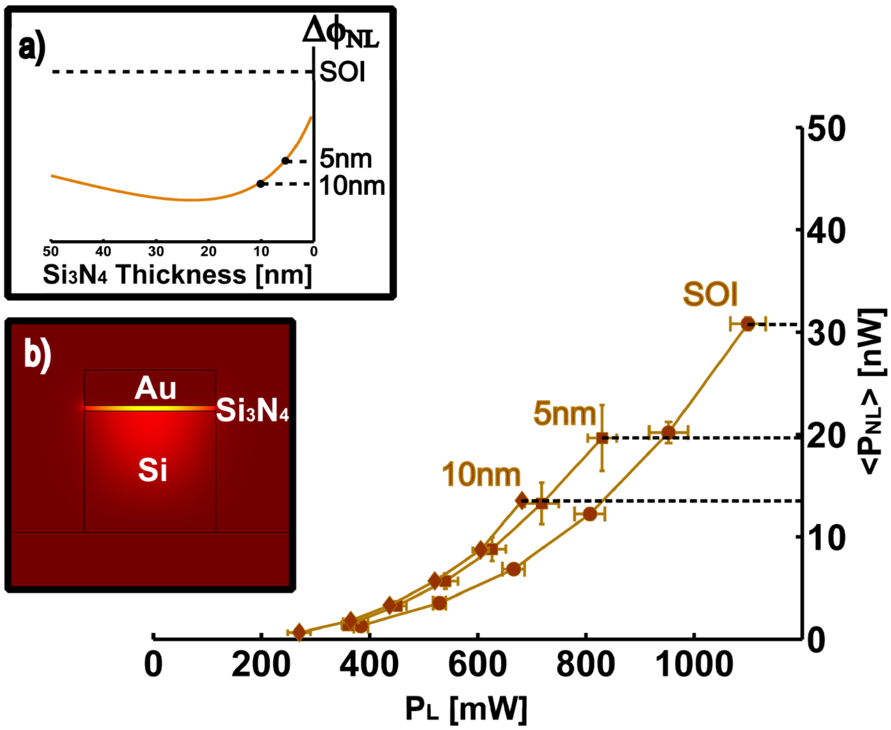

Fig. 5. Nonlinear signal generated by an SOI waveguide control and two HPWG structures of differing Si_3N_4 thickness: 10nm and 5nm. All waveguides are 10 μm in length. a) Theoretical nonlinear phase shift (with P = 1000 mW and L = 10 μm) of the SOI waveguide and HPWG as a function of Si_3N_4 thickness. b) HPWG cross-section overlapped with TM fundamental mode power profile.

It is clear the nonlinear signal generated by the SOI waveguide is larger than in the HPWGs for equal input power. However, the 5 nm HPWG generates a nonlinear signal that is stronger than the 10 nm HPWG. Inset Fig. 5a shows the theoretical phase shift expected from the HPWG versus Si_3N_4 thickness, calculated by considering the fundamental mode and including propagation losses. The qualitative agreement between the theoretical calculations and experimental data show that the method can detect the nonlinear potential of HPWGs.

Although the field intensity is higher in the Si_3N_4, our current HPWG design cannot beat conventional silicon nanowires. We note two factors; the propagation losses of the HPWG is large enough to hinder nonlinear phase shift accumulation, and Si_3N_4 possesses a lower

#253928 Received 17 Nov 2015; revised 18 Dec 2015; accepted 20 Dec 2015; published 7 Jan 2016

nonlinear refractive index than silicon. Perhaps by replacing the Si_3N_4 material with a highly nonlinear polymer, which possesses both a low refractive index and a high $\chi^{(3)}$ [35], the hybrid structure may yet fulfill its promise for enhanced nonlinearity.

4. Conclusions

We have demonstrated that our background-free method is extremely sensitive and capable of observing small differences in nonlinearity between two extremely short SOI waveguides. Our technique allows us to measure and distinguish a nonlinear phase shift as small as $7.9 \cdot 10^{-4}$ rad. To our knowledge this is the smallest measured nonlinear phase shift to date. We stress that the high sensitivity serves an advantage when measuring the nonlinear parameters associated with novel plasmonic waveguide structures. Traditional methods are hindered as the high losses associated with plasmons make measuring long accumulated phase shifts nearly impossible. With this technique we will be able to add experimental evidence to better understand the true potential of HPWG structures which are currently being considered as potential candidates for nonlinear optical applications.

Furthermore we have performed the first experimental intra-pulse 4WM measurements on hybrid plasmonic waveguides. This experimental validation is the first building block to promote further investigations on HPWGs. By engineering the design to augment the nonlinear parameter and minimize propagation losses, the hybrid plasmonic platform could potentially become competitive.

Acknowledgements

We thank NSEC for fabricating and providing the samples. We also acknowledge the equipment support provided by Coherent Inc. and Princeton Instruments. This work was funded by the Australian Research Council (Discovery Projects scheme, DP150100779) and supported by U.S. Air Force Office of Scientific Research (AFOSR) MURI program (Grant FA9550-12-1-0024).